Proximity Effects in Bilayer Graphene on Monolayer WSe_2: Field-Effect Spin Valley Locking, Spin-Orbit Valve, and Spin Transistor

Martin Gmitra and Jaroslav Fabian
Institute for Theoretical Physics, University of Regensburg, 93040 Regensburg, Germany
(Received 16 June 2017; published 4 October 2017)

Proximity orbital and spin-orbit effects of bilayer graphene on monolayer WSe_2 are investigated from first principles. We find that the built-in electric field induces an orbital band gap of about 10 meV in bilayer graphene. Remarkably, the proximity spin-orbit splitting for holes is 2 orders of magnitude—the spin-orbit splitting of the valence band at K is about 2 meV—more than for electrons. Effectively, holes experience spin valley locking due to the strong proximity of the lower graphene layer to WSe_2. However, applying an external transverse electric field of some 1 V/nm, countering the built-in field of the heterostructure, completely reverses this effect and allows, instead of holes, electrons to be spin valley locked with 2 meV spin-orbit splitting. Such a behavior constitutes a highly efficient field-effect spin-orbit valve, making bilayer graphene on WSe_2 a potential platform for a field-effect spin transistor.

DOI: 10.1103/PhysRevLett.119.146401

Introduction.—Heterostructures of two-dimensional materials can fundamentally alter their properties due to proximity effects. For example, graphene on transition metal dichalcogenides (TMDCs) can serve as a new platform for optospintronics [1], as recently was also demonstrated experimentally [2,3] promoting graphene spintronics [4] towards applications [5,6]. Bilayer graphene (BLG) on TMDCs is expected to represent an even more technologically feasible approach as it allows a precise (sub-meV) control of the chemical potential—due to much smaller Fermi level fluctuations [7]—than in single layer graphene [8].

There have recently been intensive efforts to predict realistic graphene structures, through enhancing spin-orbit coupling by decorating graphene with adatoms, that would exhibit quantum spin (and anomalous) Hall effects [9–12], introduced by Kane and Mele [13] as a precursor of topological insulators [14–16]. Unlike promising approaches to enhance spin-orbit coupling via adatoms [17,18], demonstrated already experimentally by the giant spin Hall effect signals [19,20], van der Waals heterostructures provide more robust control towards technological reproducibility of devices. Recently, proximity effects in graphene on the whole family of TMDCs as potential substrates for graphene were explored theoretically [21,22]. An enhancement of proximity spin-orbit coupling, of about 1 meV, was predicted, which is giant compared to bare graphene, in which spin-orbit coupling is about 10 μeV [23]. The special case is graphene on WSe_2, where the predicted band inversion was proposed to lead to novel topological properties [22,24,25], and giant spin relaxation anisotropy [26]. Importantly, graphene/TMDCs have already been grown [27–30] and investigated for transport [20,24,31–34], and for optoelectronics [35], as well as considered for technological applications [36–39].

BLG can exhibit an electronic band gap in the presence of a transverse electric field [40–43]. The tunable band gap enables a variety of different device concepts with novel functionalities for electronic, optoelectronic, and sensor applications. There were several proposals to increase the on-to-off ratio in gated BLG, introducing a tunnel field-effect transistor [44] or a field-effect transistor by adsorbate doping [45] to establish a displacement field. Also, BLG/TMDC heterostructures can potentially realize predicted topological insulating phases protected by no-valley mixing symmetry, featuring quantum valley Hall effects and chiral edge states [46–48].

In this Letter we find, by performing first-principles investigations, that in a BLG/WSe_2 heterostructure, shown in Fig. 1, a displacement field emerges intrinsically, allowing for a highly efficient electric control of proximity effects. Specifically, we find the following. (i) The intrinsic band gap, which is about 10 meV, can be enhanced, reduced to zero, or reversed by typical experimental electric fields on the order of 1 V/nm. (ii) The spin-orbit coupling of the valence band is giant, about 2 meV, being 2 orders of magnitude greater than in the conduction band, which is similar to intrinsic BLG [49]. The reason for this huge disparity is that the valence band is formed by nondimer carbon atom orbitals in the bottom layer adjacent to WSe_2, while the conduction band is formed by nondimer orbitals in the top layer, where proximity effects are naturally weak (the pair of atoms vertically connected we call a dimer, the other pair a nondimer). (iii) The spin-orbit coupling of the valence bands is of spin valley locking character, inherited from the monolayer WSe_2 substrate. (iv) A transverse electric field can turn spin-orbit coupling and spin valley locking of electrons effectively on (and holes off), by countering the built-in field. We call this effect the spin-orbit valve. Connecting the spin-orbit coupling to spin relaxation, the two decades of spin-orbit coupling translate into a 4 orders of magnitude change in spin relaxation.

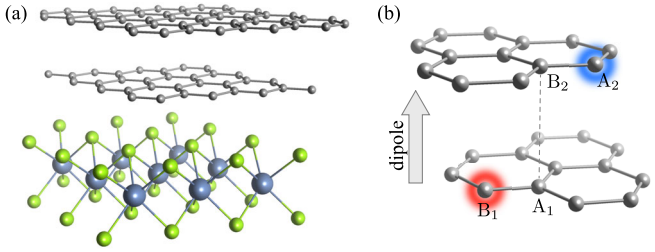

FIG. 1. (a) Atomic structure of bilayer graphene on monolayer WSe_2 (supercell). (b) Sketch of bilayer graphene with atom labels forming a bare unit cell in Bernal stacking. Orbitals on nondimer atoms B_1 and A_2 form the low energy valence and conduction bands in the electronic structure of bilayer graphene, with B_1 being closer to WSe_2.

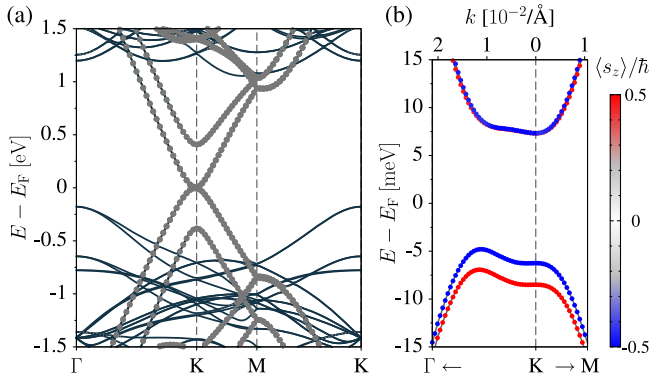

FIG. 2. (a) Calculated electronic band structure of bilayer graphene on monolayer WSe_2. Bilayer graphene π conjugated states are emphasized by the gray circles. (b) Enlargement to the fine structure of the low energy bands close to the Fermi level. Bands with a positive (negative) z component of the spin are shown in red (blue).

Such a strong field-effect spin relaxation effect would be an ideal platform for the spin transistor of Hall and Flatte [50].

Electronic band structure of bilayer graphene on WSe_2.—The electronic structure calculations and structural relaxation were performed by QUANTUM ESPRESSO [51], see the Supplemental Material [52] for further details [53–57]. In Fig. 2(a) we show the calculated electronic band structure of BLG on monolayer WSe_2 along high symmetry lines. The parabolic band dispersion of high and low energy bands close to the Fermi level resembles bare BLG [43,58]. The high energy bands originate from the orbitals in dimer A_1 and B_2 atoms connected by direct interlayer hopping [43,58], which shifts the bands some 400 meV off the Fermi level, far enough to ignore these bands for transport.

The proximity effects influence mainly the low energy bands of BLG. These bands originate from the p_z orbitals on nondimer B_1 and A_2 atoms, which form the valence and conduction band edges, respectively. An indirect band gap of 12 meV, see Fig. 2(b), is opened due to the proximity induced intrinsic electric field built across the BLG/WSe_2 heterostructure. The transverse field points from WSe_2 towards the BLG (we call this direction positive) with the amplitude of 0.267 V/nm. This is why B_1 electrons have lower energy, and form the valence band, while A_2 electrons have higher energy and form the conduction band. Apart from the orbital effect, the proximity also induces significant spin splitting of 2.2 meV in the valence band, seen in Fig. 2(b). This makes sense as B_1 atoms, responsible for the valence band, are close to WSe_2 and experience the proximity effects most.

Proximity effects in the conduction band are essentially nonexistent, since A_2 atoms sit far from WSe_2. The numerical value of the spin-orbit splitting for the conduction band obtained by QUANTUM ESPRESSO is too small (about 3 μeV), as d orbitals are not properly treated by the method. We know that in pristine BLG spin-orbit splitting should be about 24 μeV, due to the presence of d orbitals [49]. We can safely assume that this value (perhaps up to 10% higher or lower due to the proximity effects on p orbitals) of spin-orbit splitting is there for BLG on WSe_2. We conclude that holes experience spin-orbit coupling (2 meV) 2 orders of magnitude higher than electrons (20 μeV). A recent experiment has observed Shubnikov–de Haas oscillations in BLG on WSe_2 and has found, by fitting the results to a simple band structure model, that the spin-orbit proximity effect is about 10 meV [59]. Our results presented here disagree with this interpretation.

Valley spin-orbital effects.—Inspecting energy dispersions near the K valley for the spin split low energy bands, we find pronounced trigonal warping, see the color map plots in the k_x and k_y momentum plane in Figs. 3(a) and 3(c). Only the bottom spin-orbit split conduction band and the top valence bands are shown. The area of the plots corresponds to 0.5% of the full first Brillouin zone. The calculated spin expectation values for the low energy states are principally locked out of plane, see the color map plots in Figs. 3(b) and 3(d).

For low carrier concentrations, the Fermi contours form three pockets along the K–Γ directions. Further increase of doping level merges the three Fermi pockets with an emerging pocket centered at the K point. The change in Fermi surface topology is referred to as the Lifshitz transition [60], which was studied previously in bare bilayer graphene [61]. For the top valence band the merging occurs at the carrier concentration of 0.064×10^{12} cm^{-2}. This is accompanied by the presence of a van Hove singularity in the density of states [52]. The same holds for the spin-orbit split band. The second van Hove singularity appears at the energy lower by 2.2 meV, which corresponds to the proximity induced spin-orbit splitting. A further increase of the Fermi level leads to a linear increase of the Fermi surface area and carrier concentrations [52]. Multiplying the calculated carrier concentration [52] by $h/2e$ we can estimate the inverse frequency of the Shubnikov–de Haas oscillations, which for carrier

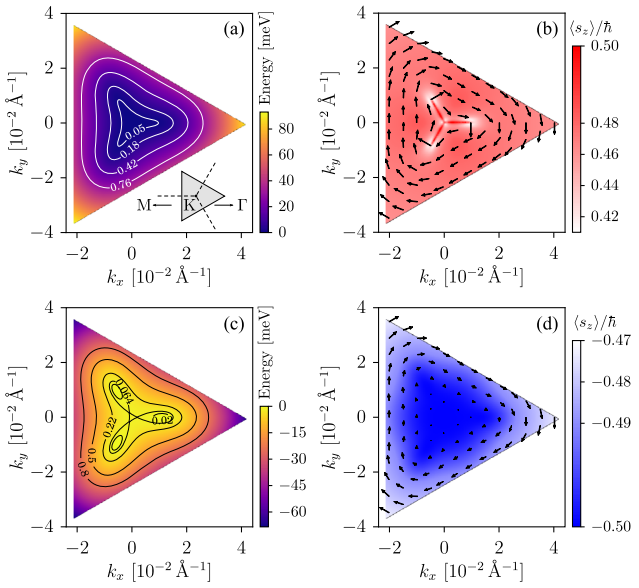

FIG. 3. Calculated low energy electronic and spin properties of bilayer graphene on monolayer WSe_2. Shown are color map plots centered at the K point representing 0.5% of the first Brillouin zone area for (a) the energy of the bottom conduction band measured from the conduction band edge. The contours correspond to carrier concentrations for 0.05, 0.18, 0.42, and 0.76×10^{12} cm^{-2}. The inset depicts a cut of the first Brillouin zone, shown by dashed lines, near the K point with directions towards M and Γ points. (b) Color map of the z component spin expectation value with in-plane spin textures shown by the arrows. (c) Energy of the valence band measured from the valence band edge with contours showing a carrier concentration of 0.02, 0.064, 0.22, 0.5, and 0.8×10^{12} cm^{-2}, and (d) similar as in (b) but for the valence band.

concentrations of about 0.2×10^{12} cm^{-2} corresponds to 10 T^{-1}. The above mentioned experiment [59] observes similar values, although we cannot make a quantitative comparison due to the absence of carrier density data.

Spin-orbit valve.—All electrical control of spin and orbital properties is a key feature for spintronics devices. Proximity induced spin-orbit coupling and the intrinsic electric polarization in a BLG/WSe_2 heterostructure can be efficiently controlled by an applied transverse electric field, as shown in the plot of low energy band structures of BLG in the presence of applied electric fields in Fig. 4. Spontaneous polarization of the heterostructure induces a dipole in the simulated cell of about 0.7D. This gives rise to a built-in transverse electric field of 0.267 V/nm, which opens the electronic band gap in BLG to the value of 12 meV. Applying a positive electric field the electronic gap further opens as the external field adds to the built-in internal field, see Fig. 4(e). However, when the applied field direction is reversed, the band gap shrinks, and for the field of −0.25 V/nm, which nearly compensates the intrinsic field, the gap fully closes, see Fig. 4(c). A further decrease (increase of the negative amplitude) of the field opens the band gap again, but the characters of the valence and conduction bands flip and we get a spin-orbit valve.

The reason for this effect is simple. At a zero applied electric field the spin-orbit splitting of the low energy valence bands originates from the bottom layer of BLG, adjacent to WSe_2. More specifically, as already mentioned, the bands originate from the orbitals on carbon atoms B_1. On the contrary, the low energy conduction bands are localized on the top (remote) BLG layer, specifically on atoms A_2, see Fig. 4(d). The spin-orbit splitting of the valence bands is about 100 times larger near the K valley in comparison to the conduction band splitting. In the built-in electric field the bottom BLG layer experiences a lower potential than the top layer. Therefore, the valence (occupied) states originate from the bottom BLG layer, and the conduction (unoccupied) states from the top layer. For a negative applied field of −0.5 V/nm the potential across the BLG reverses and the band character switches, compare Figs. 4(a) and 4(d). Applying the external electric field

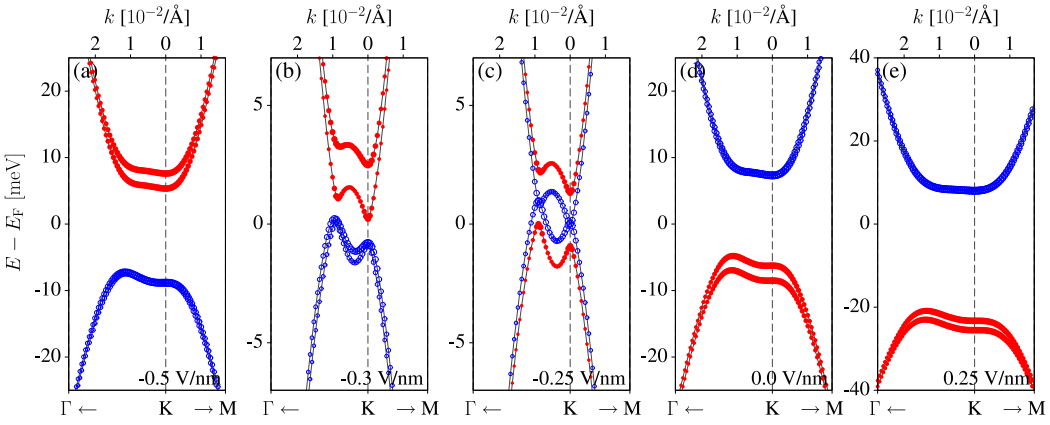

FIG. 4. Calculated sublattice resolved band structures around the K valley for a transverse electric field of (a) −0.5 V/nm, (b) −0.2979 V/nm, (c) −0.25 V/nm, (d) a zero field, and (e) 0.25 V/nm. The circle radii correspond to the probability of the state being localized on carbon atoms B_1 [(red) filled circles] and atoms A_2 [(blue) open circles].

induces also changes in the energy offset of the low energy bands with respect to the valence band maximum of the WSe_2. For negative fields the BLG valence top is pushed down in energy and for the fields below -1 V/nm the valence top of the WSe_2 is above the valence top of BLG. In effect, BLG gets electron doped [52].

Bilayer graphene spin transistor.—The proposed electrical switching of the spin-orbit splitting (either by changing the doping between electrons and holes, or by changing the electric field at a fixed chemical potential) presents a unique opportunity for a novel spin transistor design. We build on the spin transistor proposed by Hall and Flatte [50], which is an alternative to charge-based transistors, by overcoming the k_BT barrier for on-off operations.

Suppose we have a half-metallic spin injector and detector, in an antiparallel configuration, connected to BLG proximitized to a TMDC, see Fig. 5. We can control the spin-orbit coupling of the carriers in BLG by the spin-orbit valve effect. In the on state, the spin-orbit coupling is high, spin relaxation is fast, and the spin in the channel is reduced. Large current flows. In the off state, spin-orbit coupling is weak, spin relaxation slow, and the spin in the channel is preserved. No current (in the ideal case) flows.

The reason why this works is that spin relaxation depends on the square of the spin-orbit coupling. BLG on WSe_2 should have spin relaxation due to the D'yakonov-Perel effect [62], which is a motional narrowing of the spin precession in a fluctuating (due to momentum scattering) emerging spin-orbit field $\mathbf{\Omega}(k)$. The spin-orbit splitting energy is proportional to $\hbar\Omega$, where Ω is the averaged spin-orbit field for a Fermi contour. The spin relaxation rate is then given by $1/\tau_s = \Omega^2\tau$, where τ is the momentum relaxation time. Having calculated spin splitting at a zero field of 2.2 meV for the low energy bands, we estimate the spin relaxation time of 1 ps, assuming typical value for $\tau = 100$ fs. Applying an electric field of -0.5 V/nm, the band character switches and the spin relaxation is reduced, which is comparable to what is seen in ultraclean graphene [63,64] and BLG [65] encapsulated in hexagonal boron nitride. The expected field-effect variation of the spin relaxation time in BLG on WSe_2 is 4 orders of magnitude. Such a modulation is, to the best of our knowledge, unprecedented.

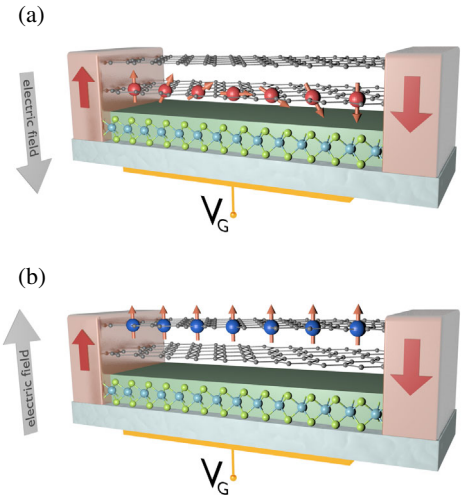

FIG. 5. Schematics of a spin-field effect transistor of bilayer graphene on a transition metal dichalcogenide with two ferromagnets in antiparallel configuration acting as the injector and detector of spins in the (a) spin-on and (b) spin-off state.

In conclusion, we have studied from first principles the electronic structure of bilayer graphene on WSe_2. The most important finding is the field-effect spin-orbit valve, allowing for an efficient switching, by 2 orders of magnitude, of the spin-orbit coupling of electrons and holes.

This work was supported by DFG SFB 689 and SFB 1277, and by the European Union's Horizon 2020 research and innovation program under Grant Agreement No. 696656. The authors gratefully acknowledge the Gauss Center for Supercomputing e.V. for providing computational resources on the GCS Supercomputer SuperMUC at the Leibniz Supercomputing Center.

[1] M. Gmitra and J. Fabian, Phys. Rev. B **92**, 155403 (2015).
[2] A. Avsar, D. Unuchek, J. Liu, O. L. Sanchez, K. Watanabe, T. Taniguchi, B. Ozyilmaz, and A. Kis, arXiv:1705.10267.
[3] Y. K. Luo, J. Xu, T. Zhu, G. Wu, E. J. McCormick, W. Zhan, M. R. Neupane, and R. K. Kawakami, Nano Lett. **17**, 3877 (2017).
[4] W. Han, R. K. Kawakami, M. Gmitra, and J. Fabian, Nat. Nanotechnol. **9**, 794 (2014).
[5] I. Žutić, J. Fabian, and S. Das Sarma, Rev. Mod. Phys. **76**, 323 (2004).
[6] J. Fabian, A. Matos-Abiague, C. Ertler, P. Stano, and I. Žutić, Acta Phys. Slovaca **57**, 565 (2007).
[7] G. M. Rutter, S. Jung, N. N. Klimov, D. B. Newell, N. B. Zhitenev, and J. A. Stroscio, Nat. Phys. **7**, 649 (2011).
[8] J. Martin, N. Akerman, G. Ulbricht, T. Lohmann, J. H. Smet, K. von Klitzing, and A. Yacoby, Nat. Phys. **4**, 144 (2008).
[9] Z. Qiao, S. A. Yang, W. Feng, W.-K. Tse, J. Ding, Y. Yao, J. Wang, and Q. Niu, Phys. Rev. B **82**, 161414 (2010).
[10] C. Weeks, J. Hu, J. Alicea, M. Franz, and R. Wu, Phys. Rev. X **1**, 021001 (2011).
[11] H. Zhang, C. Lazo, S. Blügel, S. Heinze, and Y. Mokrousov, Phys. Rev. Lett. **108**, 056802 (2012).
[12] Z. Qiao, W. Ren, H. Chen, L. Bellaiche, Z. Zhang, A. H. MacDonald, and Q. Niu, Phys. Rev. Lett. **112**, 116404 (2014).
[13] C. L. Kane and E. J. Mele, Phys. Rev. Lett. **95**, 146802 (2005).
[14] B. A. Bernevig, T. L. Hughes, and S.-C. Zhang, Science **314**, 1757 (2006).
[15] M. König, S. Wiedmann, C. Brüne, A. Roth, H. Buhmann, L. W. Molenkamp, X.-L. Qi, and S.-C. Zhang, Science **318**, 766 (2007).

[16] H. Zhang, C.-X. Liu, X.-L. Qi, X. Dai, Z. Fang, and S.-C. Zhang, Nat. Phys. **5**, 438 (2009).

[17] A. H. Castro Neto and F. Guinea, Phys. Rev. Lett. **103**, 026804 (2009).

[18] M. Gmitra, D. Kochan, and J. Fabian, Phys. Rev. Lett. **110**, 246602 (2013).

[19] J. Balakrishnan, G. Kok, W. Koon, M. Jaiswal, A. H. C. Neto, and B. Özyilmaz, Nat. Phys. **9**, 284 (2013).

[20] A. Avsar, J. Y. Tan, T. Taychatanapat, J. Balakrishnan, G. K. W. Koon, Y. Yeo, J. Lahiri, A. Carvalho, A. S. Rodin, E. C. T. O'Farrell, G. Eda, A. H. Castro Neto, and B. Özyilmaz, Nat. Commun. **5**, 4875 (2014).

[21] T. P. Kaloni, L. Kou, T. Frauenheim, and U. Schwingenschlögl, Appl. Phys. Lett. **105**, 233112 (2014).

[22] M. Gmitra, D. Kochan, P. Högl, and J. Fabian, Phys. Rev. B **93**, 155104 (2016).

[23] M. Gmitra, S. Konschuh, C. Ertler, C. Ambrosch-Draxl, and J. Fabian, Phys. Rev. B **80**, 235431 (2009).

[24] Z. Wang, D.-K. Ki, H. Chen, H. Berger, A. H. MacDonald, and A. F. Morpurgo, Nat. Commun. **6**, 8339 (2015).

[25] B. Yang, M.-F. Tu, J. Kim, Y. Wu, H. Wang, J. Alicea, R. Wu, M. Bockrath, and J. Shi, 2D Mater. **3**, 031012 (2016).

[26] A. W. Cummings, J. H. García, J. Fabian, and S. Roche, arXiv:1705.10972.

[27] Y.-C. Lin, N. Lu, N. Perea-Lopez, J. Li, Z. Lin, X. Peng, C. H. Lee, C. Sun, L. Calderin, P. N. Browning, M. S. Bresnehan, M. J. Kim, T. S. Mayer, M. Terrones, and J. A. Robinson, ACS Nano **8**, 3715 (2014).

[28] M.-Y. Lin, C.-E. Chang, C.-H. Wang, C.-F. Su, C. Chen, S.-C. Lee, and S.-Y. Lin, Appl. Phys. Lett. **105**, 073501 (2014).

[29] M. M. Ugeda, A. J. Bradley, S.-F. Shi, F. H. da Jornada, Y. Zhang, D. Y. Qiu, W. Ruan, S.-K. Mo, Z. Hussain, Z.-X. Shen, F. Wang, S. G. Louie, and M. F. Crommie, Nat. Mater. **13**, 1091 (2014).

[30] A. Azizi, S. Eichfeld, G. Geschwind, K. Zhang, B. Jiang, D. Mukherjee, L. Hossain, A. F. Piasecki, B. Kabius, J. A. Robinson, and N. Alem, ACS Nano **9**, 4882 (2015).

[31] A. Dankert and S. P. Dash, Nat. Commun. **8**, 16093 (2017).

[32] C.-P. Lu, G. Li, K. Watanabe, T. Taniguchi, and E. Y. Andrei, Phys. Rev. Lett. **113**, 156804 (2014).

[33] S. Larentis, J. R. Tolsma, B. Fallahazad, D. C. Dillen, K. Kim, A. H. MacDonald, and E. Tutuc, Nano Lett. **14**, 2039 (2014).

[34] S. Omar and B. J. van Wees, Phys. Rev. B **95**, 081404 (2017).

[35] M. Massicotte, P. Schmidt, F. Vialla, K. G. Schdler, A. Reserbat-Plantey, K. Watanabe, T. Taniguchi, K. J. Tielrooij, and F. H. L. Koppens, Nat. Nanotechnol. **11**, 42 (2016).

[36] S. Bertolazzi, D. Krasnozhon, and A. Kis, ACS Nano **7**, 3246 (2013).

[37] K. Roy, M. Padmanabhan, S. Goswami, T. P. Sai, G. Ramalingam, S. Raghavan, and A. Ghosh, Nat. Nanotechnol. **8**, 826 (2013).

[38] W. Zhang, C.-P. Chuu, J.-K. Huang, C.-H. Chen, M.-L. Tsai, Y.-H. Chang, C.-T. Liang, Y.-Z. Chen, Y.-L. Chueh, J.-H. He, M.-Y. Chou, and L.-J. Li, Sci. Rep. **4**, 3826 (2014).

[39] N. A. Kumar, M. A. Dar, R. Gul, and J. Baek, Mater. Today **18**, 286 (2015).

[40] T. Ohta, A. Bostwick, T. Seyller, K. Horn, and E. Rotenberg, Science **313**, 951 (2006).

[41] J. B. Oostinga, H. B. Heersche, X. Liu, A. F. Morpurgo, and L. M. K. Vandersypen, Nat. Mater. **7**, 151 (2008).

[42] Y. Zhang, T.-T. Tang, C. Girit, Z. Hao, M. C. Martin, A. Zettl, M. F. Crommie, Y. R. Shen, and F. Wang, Nature (London) **459**, 820 (2009).

[43] E. McCann and V. I. Fal'ko, Phys. Rev. Lett. **96**, 086805 (2006).

[44] G. Alymov, V. Vyurkov, V. Ryzhii, and D. Svintsov, Sci. Rep. **6**, 24654 (2016).

[45] B. N. Szafranek, D. Schall, M. Otto, D. Neumaier, and H. Kurz, Nano Lett. **11**, 2640 (2011).

[46] W. Yao, S. A. Yang, and Q. Niu, Phys. Rev. Lett. **102**, 096801 (2009).

[47] F. Zhang, J. Jung, G. A. Fiete, Q. Niu, and A. H. MacDonald, Phys. Rev. Lett. **106**, 156801 (2011).

[48] L. Ju, Z. Shi, N. Nair, Y. Lv, C. Jin, J. Velasco Jr, C. Ojeda-Aristizabal, H. A. Bechtel, M. C. Martin, A. Zettl, J. Analytis, and F. Wang, Nature (London) **520**, 650 (2015).

[49] S. Konschuh, M. Gmitra, D. Kochan, and J. Fabian, Phys. Rev. B **85**, 115423 (2012).

[50] K. C. Hall and M. E. Flatt, Appl. Phys. Lett. **88**, 162503 (2006).

[51] P. Giannozzi and *et al.*, J. Phys. Condens. Matter **21**, 395502 (2009).

[52] See Supplemental Material at http://link.aps.org/supplemental/10.1103/PhysRevLett.119.146401 for details of the calculated density of states, carrier concentration, electrostatic quantities, and spin splitting of the low energy bilayer bands.

[53] J. Hohenberg and W. Kohn, Phys. Rev. **136**, B864 (1964).

[54] J. P. Perdew, K. Burke, and M. Ernzerhof, Phys. Rev. Lett. **77**, 3865 (1996).

[55] S. Grimme, J. Comput. Chem. **27**, 1787 (2006).

[56] V. Barone, M. Casarin, D. Forrer, M. Pavone, M. Sambi, and Vittadini, J. Comput. Chem. **30**, 934 (2009).

[57] L. Bengtsson, Phys. Rev. B **59**, 12301 (1999).

[58] J. Nilsson, A. H. Castro Neto, F. Guinea, and N. M. R. Peres, Phys. Rev. B **78**, 045405 (2008).

[59] Z. Wang, D.-K. Ki, J. Y. Khoo, D. Mauro, H. Berger, L. S. Levitov, and A. F. Morpurgo, Phys. Rev. X **6**, 041020 (2016).

[60] I. M. Lifshitz, Sov. Phys. JETP **11**, 1130 (1930).

[61] A. Varlet, M. Mucha-Kruczyński, D. Bischoff, P. Simonet, T. Taniguchi, K. Watanabe, V. Fal'ko, T. Ihn, and K. Ensslin, Synth. Met. **210**, 19 (2015).

[62] M. I. D'yakonov and V. I. Perel', Fiz. Tverd. Tela (Kharkov) **13**, 3581 (1971), [Sov. Phys. Solid State **13**, 3023 (1972)].

[63] M. H. D. Guimarães, P. J. Zomer, J. Ingla-Aynés, J. C. Brant, N. Tombros, and B. J. van Wees, Phys. Rev. Lett. **113**, 086602 (2014).

[64] M. Gurram, S. Omar, S. Zihlmann, P. Makk, C. Schönenberger, and B. J. van Wees, Phys. Rev. B **93**, 115441 (2016).

[65] J. Ingla-Aynés, M. H. D. Guimarães, R. J. Meijerink, P. J. Zomer, and B. J. van Wees, Phys. Rev. B **92**, 201410 (2015).